WIND ENERGY
Wind Energ. 2010; **00**:1–12
DOI: 10.1002/we

RESEARCH ARTICLE

Reduced-Order Modeling for Wind Farm Control

Jennifer Annoni, Pieter Gebraad, and Peter Seiler

ABSTRACT

Wind turbines in a wind farm operate individually to maximize their own performance regardless of the impact of aerodynamic interactions on neighboring turbines. There is the potential to increase power and reduce overall structural loads by properly coordinating turbines. To perform control design and analysis, a model of the wind farm needs to be of low computational cost, but retain the necessary dynamics seen in high-fidelity models. The objective of this work is to obtain a reduced-order model that represents the dominant dynamics of the system and maintains the appropriate input-output behavior. A variety of methods, including proper orthogonal decomposition and dynamic mode decomposition, can be used to extract the dominant flow structures and obtain a reduced-order model. In this paper, we combine proper orthogonal decomposition with a system identification technique to produce an input-output reduced-order model. This technique is used to construct reduced-order models of the flow within a two-turbine array. Specifically, this technique is demonstrated on large eddy simulations.

KEYWORDS

model reduction, wind farm control, mode decomposition

Correspondence

Journals Production Department, John Wiley & Sons, Ltd, The Atrium, Southern Gate, Chichester, West Sussex, PO19 8SQ, UK.

Received . . .

1. INTRODUCTION

In the United States, many states have a renewable portfolio standard or goal. For example, Minnesota has a renewable portfolio standard target of 25% renewable energy by 2025 [1]. Wind energy will be a significant factor in achieving this goal. Wind farm control can be used to increase wind energy efficiently by maximizing power in wind farms that are already installed. It can also be used to mitigate structural loads to maximize the lifetime of the turbines and better integrate wind energy into the energy market.

Currently, turbines in a wind farm are operated at their individual optimal operating point, which leads to suboptimal performance of a wind farm. Properly coordinating turbines has the potential to increase the overall performance of wind farms [2]. Designing wind farm control strategies requires a model of the wind farm that has a low computational cost, but retains the necessary dynamics. A variety of wake models exist in literature that are useful for studying wind farm control. The simplest model is the Park model [3]. The Park model provides a quick, preliminary description of the wake interactions in a wind farm. Various extensions of the Park model have been proposed to provide a more realistic interpretation of wind farm aerodynamics [4, 5]. Several high-fidelity computational fluid dynamics (CFD) models have been developed as well [6, 7]. These high-fidelity models are more accurate and can be used for evaluating wind farm controllers; however, they are computationally expensive. These low- and high-fidelity models have been used to evaluate wind farm control strategies [8, 9]. The analysis provides conflicting results based on the wake model chosen for control design. For example, control strategies designed using simple static models may report significant improvements in wind farm performance, but an analysis of such control strategies using high-fidelity simulation can result in minimal to no improvements in wind farm performance. An example of a comparison between control predictions given by a high-fidelity and simplified model is given in [10], where constant offsets of pitch and torque are used to change wake deficits. It is shown that extensions to the Park model are needed to match the results of high-fidelity models.

Improving models for wind farm control requires a better understanding of the aerodynamic interactions in a wind farm. Although many studies have been performed using static models and constant offsets of the operating point of the wind turbines, dynamic wake modeling and control approaches have been proposed recently. Previously proposed approaches use high-order first principle modeling by implementing the spatially filtered Navier-Stokes equations, e.g. [11], to arrive at a dynamic wake model. This paper focuses on a technique to construct a reduced-order wake model from data generated by simulations or experiments.

Techniques developed by the fluids and controls communities are relevant for reduced-order wake modeling. Some studies have been done to understand the dominant turbulent structures generated in CFD simulations and in experiment [12]. Proper orthogonal decomposition (POD) and dynamic mode decomposition (DMD) are two popular techniques in the fluids literature that compute the dominant modes of the flow [13–18]. This type of analysis has been used on wind turbine wakes [19]. These modes have been used to construct a reduced-order model that can be used for control, such as balanced POD and DMD with control (DMDc) [20–22]. Some of these methods require computing the adjoint of the system, which is not readily available in most CFD codes and is not available during experiments. The controls/systems community has an alterative set of techniques to identify models from input-output data, e.g. system identification techniques such as N4SID [23]. The methods generate reduced-order black box models to represent input-output measurements of the system. This type of reduced-order model refers to a low-dimensional representation of a high-dimensional system. In this framework, the states have no physical meaning.

In this paper, we use a method that combines system identification with POD modes that closely follows DMDc. This type of model reduction approach has two main advantages, First, it relies on input-output data from a forced response and does not require the construction/simulation of the adjoint system. Second, the reduced-order model is constructed in a way that retains the physical meaning of the states. This can be useful for parameter varying systems as is addressed in [24]. The method addressed in this paper projects the state onto a reduced-order subspace using the dominant models the system and then uses direct N4SID to define the reduced-order model for the system, described in Section 2. Section 3 describes how to handle process noise, model uncertainty, and measurement noise when using a low-dimensional model constructed from simulations or experiments. This reduced-order modeling technique is applied to simulation and experimental data of a two-turbine array, described in Section **??**, to obtain reduced-order models that capture the dominant dynamics of the system and retain the appropriate input-output behavior. This is intended to demonstrate the feasibility of this approach on simulation and experimental data. Finally, conclusions and suggestions for future work are given in Section 6.

2. INPUT-OUTPUT REDUCED-ORDER MODELING

In this section, we combine POD with system identification to produce an input-output reduced-order model (IOROM). This terminology has been used in the flexible aircraft literature to describe models of this type [25]. The proposed method closely follows the procedure used in the formulation of DMDc [22]. This approach will be summarized in this section for time-invariant systems, but has been extended to parameter-varying systems. More details can be found in [24]. The advantages of using this approach is that it produces input-output models that do not require adjoints. This paper builds on the work presented in [26].

Consider a discrete-time nonlinear system with inputs:

$$x_{k+1} = f(x_k, u_k) \tag{1}$$

$$y_k = h(x_k, u_k) \tag{2}$$

where $x \in \mathbb{R}^n$, $u \in \mathbb{R}^p$, and $y \in \mathbb{R}^q$ are the state, input, and output vectors, respectively.

A collection of snapshot measurements are obtained via simulations or experiments by exciting the system. Snapshots are taken from the nonlinear system, and the states, inputs, and outputs are recorded as:

$$X_0 = \begin{bmatrix} x_0, & x_1, & \dots, & x_{m-1} \end{bmatrix} \in \mathbb{R}^{n\times(m-1)} \tag{3}$$

$$X_1 = \begin{bmatrix} x_1, & x_2, & \dots, & x_m \end{bmatrix} \in \mathbb{R}^{n\times(m-1)} \tag{4}$$

$$U_0 = \begin{bmatrix} u_0, & u_1, & \dots, & u_{m-1} \end{bmatrix} \in \mathbb{R}^{p\times(m-1)} \tag{5}$$

$$Y_0 = \begin{bmatrix} y_0, & y_1, & \dots, & y_{m-1} \end{bmatrix} \in \mathbb{R}^{q\times(m-1)} \tag{6}$$

where m is the number of snapshots. For the wind farm example, the snapshots of the state would include the velocity at every grid point in the domain at every time step, the snapshots of the inputs would include the blade pitch angle and generator torque of each turbine in the wind farm, and the snapshots of the outputs could be the power or structural loads, e.g. tower bending, at each turbine. This method attempts to fit the snapshot measurements at a particular operating point

in time by:

$$x_{k+1} = Ax_k + Bu_k \tag{7}$$
$$y_k = Cx_k + Du_k \tag{8}$$

The dimensions of the state matrices (A, B, C, D) are compatible to those of (x, u, y). Solving this problem becomes intractable for large systems, i.e. states dimension $n > 10^5$. The state is projected onto a low-dimensional subspace to make the computations tractable.

The projection subspace is defined by a generic orthonormal basis $Q \in \mathbb{R}^{n_x \times r}$, i.e. $Q^T Q = I_r$. A reduced-order state is defined by the projection onto this basis $z := Q^T x \in \mathbb{R}^r$. A truncated model can then be expressed as follows in terms of this reduced-order state

$$\begin{aligned} z_{k+1} &= (Q^T AQ)z_k + (Q^T B)u_k := Fz_k + Gu_k \\ y_k &= (CQ)z_k + Du_k := Hz_k + Du_k. \end{aligned} \tag{9}$$

The reduced-order state matrices (F, G, H, D) are obtained by minimizing the error of the Frobenius norm using least-squares:

$$\underset{F,\,G,\,H,\,D}{\text{minimize}} \left\| \begin{bmatrix} X_1 \\ Y_0 \end{bmatrix} - \begin{bmatrix} Q & 0 \\ 0 & I_p \end{bmatrix} \begin{bmatrix} F & G \\ H & D \end{bmatrix} \begin{bmatrix} Q^T & 0 \\ 0 & I_p \end{bmatrix} \begin{bmatrix} X_0 \\ U_0 \end{bmatrix} \right\|_F^2 \tag{10}$$

This is the direct N4SID subspace method for estimating matrices given measurements of the (reduced-order) state, input, and output. A useful choice for the projection space is given by the POD modes of X_0. The POD modes can be computed using a singular value decomposition of $X_0 = U\Sigma V^T$. This is non-trivial to compute if the state dimension is very large. The SVD of X_0 can be computed using the MapReduce technique introduced in [27]. Specifically, this method is able to efficiently compute the SVD of a tall and skinny matrix, i.e. $n_x >> n_s$. The POD modes are contained in the columns of U. For additional details on POD modes, see [13–15]. The state of the reduced-order (r dimensional) system can be approximated on a subspace defined by the first r POD modes of X_0. The optimal reduced-order state matrices for this choice of $Q = U_r$ are:

$$\begin{bmatrix} F & G \\ H & D \end{bmatrix}_{\text{opt}} = \begin{bmatrix} U_r^T X_1 \\ Y_0 \end{bmatrix} \begin{bmatrix} \Sigma_r V_r \\ U_0 \end{bmatrix}^{\dagger} \tag{11}$$

where † indicates the pseudo-inverse. As with standard DMD, an eigenvalue decomposition of F_{opt} can be used to construct the dynamic modes, which provide spatial modes associated with a specific temporal frequency for the system. The F matrix describes the dynamics of the system. The G, H, and D matrices obtained using this method are computed such that the input-to-output relationship of the reduced-order model is maintained from the full-order system. This proposed method is a tractable implementation of the existing direct N4SID subspace method [23] that can be applied for very large systems. This is not simply a black-box (input-output) approach because the state of the reduced-order system z_k can be used to approximately reconstruct the full-order state by:

$$x_k \approx U_r z_k \tag{12}$$

Moreover, the approach requires state/input/output data from the model. Construction and simulation of the adjoint system is not required. It should be noted that this paper will focus on the construction of the reduced-order model rather than the evaluation of the DMD modes.

One way to choose the order r of the IOROM computed using this approach is to analyze how much energy is captured by the number of modes chosen. It is common to choose the number of modes to capture 99% of the energy (or some similar threshold) in the snapshots. However, for a sufficient model that is suitable for control, the primary metric is the amount of model error incurred from the selection of the number of modes. The model error can be computed using the Frobenius norm:

$$\left\| \begin{bmatrix} X_1 \\ Y_0 \end{bmatrix} - \begin{bmatrix} A & B \\ C & D \end{bmatrix} \begin{bmatrix} X_0 \\ U_0 \end{bmatrix} \right\|_F^2 \tag{13}$$

Again, computation of this model error is intractable for systems with extremely large state dimension. However, the properties of the Frobenius norm can be used to equivalently rewrite this error in a more useful form:

$$\left\| \begin{bmatrix} X_1 \\ Y_0 \end{bmatrix} - \begin{bmatrix} A & B \\ C & D \end{bmatrix} \begin{bmatrix} X_0 \\ U_0 \end{bmatrix} \right\|_F^2 = \left\| \begin{bmatrix} Q^T X_1 \\ Y_0 \end{bmatrix} - \begin{bmatrix} F & G \\ H & D \end{bmatrix} \begin{bmatrix} Q^T X_0 \\ U_0 \end{bmatrix} \right\|_F^2 + \|X_1\|_F^2 - \left\| Q^T X_1 \right\|_F^2 \tag{14}$$

The first term represents the model error on the projected subspace. The second and third terms represent the energy lost in the snapshot data X_1 by using the projection. The right hand side of this equation is now tractable because the

states are projected onto a subspace and have dimension r. More importantly, only the reduced-order state matrices, i.e. (F, G, H, D), are needed for the calculation rather than the full states matrices (A, B, C, D). In many fluid dynamic examples, it is infeasible to compute A, which would have dimensions of $10^6 \times 10^6$. Increasing the number modes will generally decrease the total error. However, there is a point when adding additional modes will not significantly improve the model error. In fact, adding the modes beyond this point could result in a model that is trying to overfit the nonlinearities in the system resulting in a degradation of the performance.

It is important to note that this approach for computing the model error is dominated by the state dimension rather than focusing on fitting the input-output behavior. Future work will include a weighted approach to computing the error to focus the model fit on the input-output behavior.

3. INPUT-OUTPUT REDUCED-ORDER MODEL WITH A KALMAN FILTER

To apply this IOROM approach to higher fidelity simulations or experiments, a way to handle the error between the reduced-order model and the nonlinear simulation/experiment is introduced in this section. Note that the IOROM identified, using the technique described in Section 2, is the best fit model for the available data. For example, one issue that arises in high-dimensional systems is the influence of turbulence. This is a disturbance in the system that cannot exactly be quantified in a linear, time invariant model. The IOROM method is useful in identifying the dominant dynamics and maintaining the approximate input-output behavior. To improve the performance of the model, it is recommended that state estimator be used along with the IOROM to handle the influence of disturbances, such as turbulence. For this study, a Kalman filter will be used with the identified IOROM [28, 29]. This is standard practice in the controls/system literature. An example of combining an analytically derived parameteric wind farm model with a Kalman filter to account for the influence of turbulence is given in [30]. A more similar approach was proposed in [31] where a model constructed using DMD and this model was embedded in a Kalman filter. The Kalman filter is the best linear filter for a system even if the noise is not Gaussian [28]. Any improvements over the Kalman filter would require a nonlinear filter. The Kalman filter is able to provide a computationally efficient algorithm for estimating the state based on measured outputs. It should also be reiterated that the purpose of this Kalman filter is aid the IOROM in predicting the dominant characteristics rather than the turbulent characteristics of the flow. The IOROM embedded in the Kalman filter is briefly described in this section.

Consider the reduced-order model of the system with noise

$$\begin{aligned} z_{k+1} &= Fz_k + Gu_k + w_k \\ y_k &= Hz_k + Du_k + v_k \end{aligned} \tag{15}$$

where $w_k \in \mathbb{R}^r$ is the process noise and $v_k \in \mathbb{R}^{n_y}$ is the measurement noise. For the wind farm example, z_k are the POD modes of the system, u_k are the inputs such as blade pitch angle and generator torque, and y_k are the measurements of the wind farm such as the power of each turbine, wind speed, or structural loads.

The standard Kalman filter can be implemented with the IOROM using the approach outlined in [29]. The Kalman filter uses measurements to update the estimate of the state at a particular time step. To implement the Kalman filter, the properties of the process noise w_k and measurement noise v_k should be known or estimated. Typically, the covariance matrices of the process noise, Q_k, and measurement noise, R_k, can be determined by $Q_k = E(w_k w_k^T)$ and $R_k = E(v_k v_k^T)$. This indicates that the process noise and measurement noise are independent. However, in the wind farm application, the information about the noise is not known. Hence Q_k and R_k are tuned to estimate the noise. Especially for wind farm simulations, R_k is expected to be small since exact measurements can be taken from the simulations. Q_k is tuned such that all of the modes of the reduced-order model are weighted equally. Another approach to defining Q_k could be to weight the modes differently, e.g. assign higher weights to the less dominant modes. The Kalman filter is initialized by

$$\begin{aligned} \hat{z}_0^+ &= E(z_0) \\ P_0^+ &= E[(z_0 - \hat{z}_0^+)(z_0 - \hat{z}_0^+)^T], \end{aligned}$$

where z_0^+ is the initial state estimate and P_0^+ is the covariance on the state error. For these wind farm examples addressed in this paper, the initial covariance, P_0^+, is set to be I_r. The remainder of the Kalman filter is evaluated as

$$\begin{aligned} \text{Covariance:} \quad & P_k^- = FP_{k-1}^+F^T + Q_{k-1} \\ \text{Kalman Gain:} \quad & K_k = P_k^- H^T (HP_k^- H^T + R_k)^{-1} \\ \text{State Estimate:} \quad & \hat{z}_k^- = F\hat{z}_{k-1}^+ + Gu_{k-1} \\ \text{Measurement Update:} \quad & \hat{z}_k^+ = \hat{z}_k^{-1} + K_k(y_k - H\hat{z}_k^- - Du_k) \\ \text{Covariance Update:} \quad & P_k^+ = (I - K_k H)P_k^- \end{aligned}$$

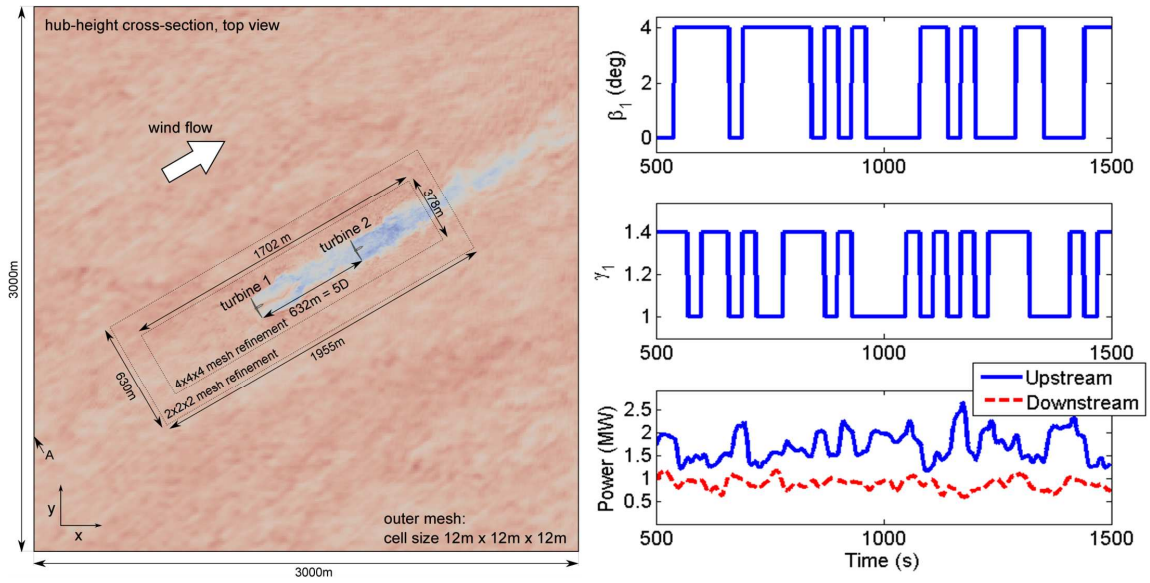

Figure 1. (Left) Setup for the two-turbine array in SOWFA. (Right) Forced input used for the two-turbine array.

where "$^-$" indicates the settings of the filter before the measurement update and "$^+$" indicates after the measurement update. This approach shows good performance when used with the identified IOROM. Note that the performance of the Kalman filter is dependent on the model identified by the IOROM approach. Specifically, if the selected model has too many modes, the IOROM is essentially overfitting the data. Although this may provide a good performance with the data the model originated from, the model shows poor performance even with a Kalman filter implemented, i.e. the Kalman filter has to compensate significantly to fit a different data set of the same properties. An example of this is shown in the results section.

Other filter approaches have been investigated including the $\mathcal{H}_\infty$ filter [29] where there is no assumption on noise and they show similar performance. Future work will address the advantages and disadvantages of using a Kalman filter over other filter processes.

4. LARGE EDDY SIMULATIONS

The IOROM method was used to obtain a reduced-order model from the Simulator fOr Wind Farm Applications (SOWFA) simulations [6]. SOWFA is a high-fidelity large eddy simulation tool that was developed at the National Renewable Energy Laboratory (NREL) for wind farm studies. SOWFA is a CFD solver based on OpenFOAM and is coupled with NREL's FAST modeling tool [32]. SOWFA has been used in previous wind farm control studies [8, 33]

SOWFA uses an actuator line model coupled with FAST to study turbines in the atmospheric boundary layer. Specifically, SOWFA solves the three-dimensional incompressible Navier-Stokes equations and transport of potential temperature equations, which take into account the thermal buoyancy and Earth rotation (Coriolis) effects in the atmosphere. The inflow conditions for this simulation are generated using a periodic atmospheric boundary layer precursor with no turbines. Additional details can be found in [8].

SOWFA calculates the unsteady flow field to compute the time-varying power, velocity deficits, and loads at each turbine in a wind farm. This level of computation, with high-fidelity accuracy, takes a number of days to run on a supercomputer using a few hundred to a few thousand processors, depending on the size of the wind farm. The simulations run for this study were performed on NREL's high-performance computer Peregrine.

4.1. Two-Turbine Setup

A high-fidelity simulation of a two-turbine scenario was performed with SOWFA to provide the data for the IOROM. The two-turbine setup is shown in Figure 1 (left). The turbines were aligned with the dominant wind direction with a spacing of 5 diameters (5D). The simulated turbines are NREL 5 MW baseline turbines [34], which have a rotor diameter of D = 126 m. The conditions simulated in SOWFA are based on the study reported in [8, 33]. They consist of a neutral

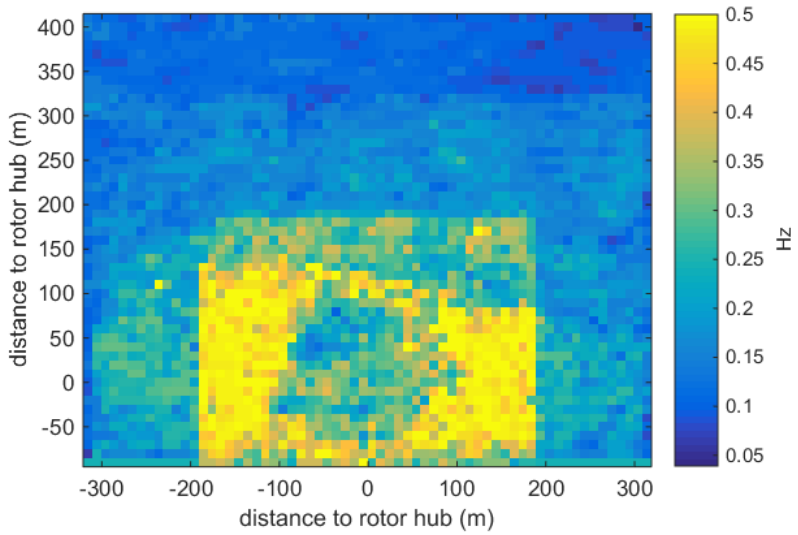

Figure 2. Frequency content of the flow velocity field at 4D downstream of the upstream turbine. Specifically, this shows the -20dB bandwidth of the fast Fourier transform of the velocity signal for saple points at 4D downstream. Note that the velocity signal was sampled at 1Hz. The pure yellow may indicate that the frequency at these points exceeds 0.5Hz.

atmospheric boundary layer with a low aerodynamic surface roughness value of 0.001 m, which is typical for offshore conditions. The generated inflow, coming from the southwest (300°), has a horizontally averaged wind speed of 8 m/s and a turbulence intensity of 10 % at the turbine hub height. A simulation time of 1800 s is used to let the wakes develop through the domain. The spatial discretization for the CFD solver is refined in two steps with the smallest cells containing the turbine rotors, the axial induction zones of the rotor, and a large part of the wake. Farther from the turbines, the mesh is coarser to reduce computation time.

4.2. IOROM with SOWFA

The IOROM method can be used to construct a reduced-order model of the two-turbine setup. For this particular example, there are four inputs: the blade pitch angle (β_1) and the generator torque (τ_{g1}) of the upstream turbine and the blade pitch angle (β_2) and the generator torque (τ_{g2}) of the downstream turbine. In this example, the generator torque is modulated by changing a scaling constant associated with the standard generator torque control law for Region 2 operation of a utility-scale turbine [35]. Specifically, the scaling factor, γ, is applied to the generator torque control law of the upstream turbine, so that the applied generator torque is $\tau_g = \gamma K_g \omega^2$ with $K_g = 0.0179\,\text{Nm/RPM}^2$ and ω is the rotor speed [RPM], resulting in a deviation from the turbine-level optimal gain K_g for maximum power production. The outputs of interest are the power generated by the upstream (P_1) and downstream turbine (P_2). Overall, the goal is to generate a reduced-order model of this form:

$$\begin{aligned} z_{k+1} &= Fz_k + Gu_k \\ y_k &= Hz_k + Du_k \end{aligned} \tag{16}$$

where $u := [\beta_1, \gamma_1, \beta_2, \gamma_2]$ and $y := [P_1, P_2]$.

To generate an IOROM of this example, forced inputs were applied to the upstream turbine by changing the collective blade pitch angle from 0° to 4° using a pseudo-random binary sequence (PRBS), see the top plot in Figure 1 (right). In addition, the generator torque constant, γ_1, was modulated between 1 and 1.4 using a different PRBS, see the middle plot in Figure 1 (right). The blade pitch angle and generator torque constant of the downstream turbine were held at constant at their optimal values, i.e. $\beta_2 = 0$ and $\gamma_2 = 1$, see the bottom plot in Figure 1 (right). This indicates how the forcing inputs at the upstream turbine affect the power output of both the upstream and downstream turbines. By changing the blade pitch angle and generator torque constant at varying frequencies, various dynamics of the system are excited.

The data from the simulations were sampled at 1 s intervals, i.e. snapshots from the flow are recorded every 1 s. The sampling time was determined by doing a frequency analysis of the flow in a two-turbine array. In particular, Figure 2 shows that a majority of the frequency content in the rotor swept area (63 m around the orgin) of the wake is of lower frequency, i.e. less than 0.5 Hz. There is higher frequency at the edges of the wake due to the presence of a shear layer. For

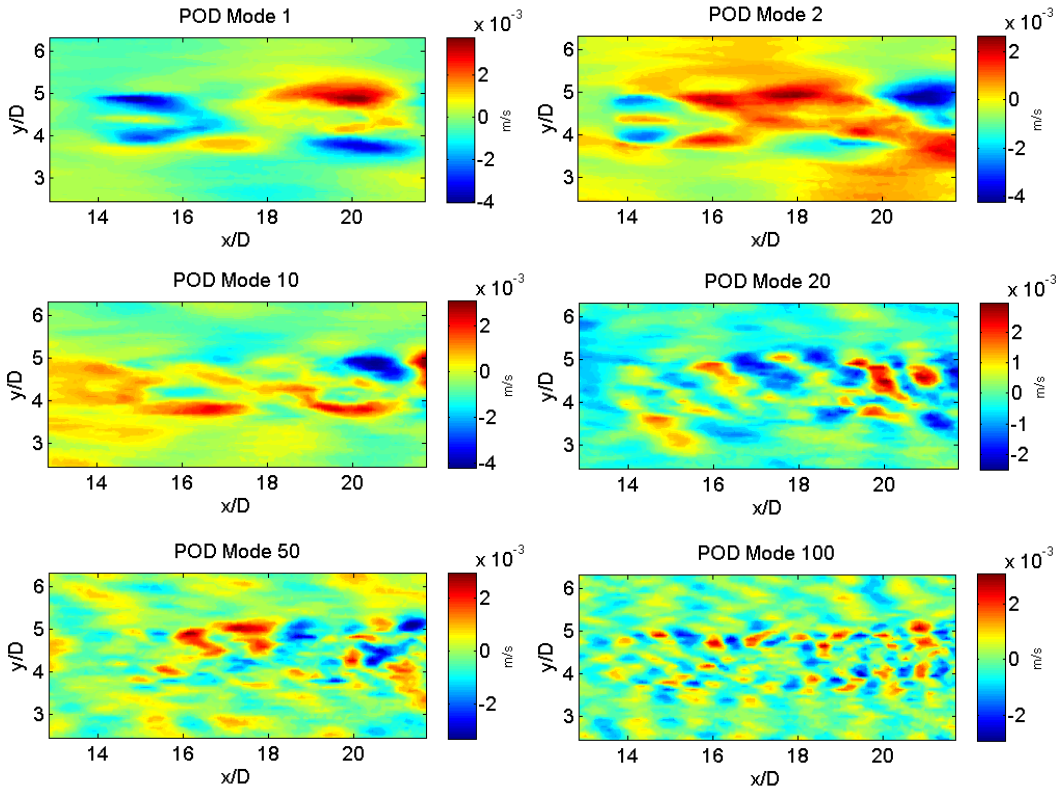

Figure 3. POD modes 1, 2, 10, 20, 50, and 100 of the SOWFA simulation. Mode 1 is the mode of the system with the largest amount of energy, typically corresponding to low spatial frequency components of the system. Mode 100 captures less energy in the system as is typically associated with higher spatial frequency components.

this analysis, it should be noted that the Fast Fourier Transform in Figure 2 is based on 1 Hz data. The Nyquist frequency is thus 0.5 Hz. Much of the information in the wake has a lower frequency than 0.5 Hz. It should also be noted that nothing definitive can be said about higher frequencies with this analysis. However, to capture the dominant characteristics of the system, i.e. the dynamics with lower frequencies, it appears that a 1 Hz sampling rate is sufficient for the construction of the IOROM based on SOWFA simulations.

The time step of the SOWFA simulation is 0.01 s. To collect data for 1800 s, this would amount to 180,000 snapshots of data. This is impractical to store and analyze. As a result, only one snapshot of the flow is taken per 100 simulation time steps. The resulting IOROM will be a discrete time model with a time step of 1 s.

5. RESULTS

The results shown in this section were obtained using the IOROM constructed from data from the simulation scenario described in the previous sections. Note that the resulting flow field plots have been rotated in this section so that the flow is shown moving from left to right. The upstream and downstream turbines are indicated by black lines in the flow field figures in this section.

To construct the IOROM, the flow in the two-turbine array was sampled at 1.2 million grid points in the SOWFA simulations. Specifically, the three velocity components were recorded at each grid point resulting in 3.6 million states. The velocities are stacked into a single vector and collected in a snapshot matrix, X_0. Similarly, the inputs $(\beta_1, \gamma_1, \beta_2, \gamma_2)$ and outputs (P_1, P_2) are recorded at each IOROM time step. The POD modes of the snapshot matrix, X_0, were computed using the MapReduce approach presented in [27]. The IOROM was constructed with 1000 snapshots at 1 s intervals for a total time of 1000 s. This indicates that the lowest frequency that this IOROM could capture is on the order of 10^{-3}. Figure 3 shows the POD modes 1, 2, 10, 20, 50, and 100 of the streamwise velocity component at hub height (90 m). The POD modes are used to project the system onto a low-dimensional subspace such that direct N4SID can be used to identify a low-order model of the wind farm. It should be noted that these modes were computed after subtracting out the

baseflow. As a result, the IOROM can be thought of as a linear model that represents the fluctuations about an equilibrium point, or mean flow. The first mode contains low-frequency spatial information and is the most energetic mode of the system. Mode 100 has high-frequency spatial information and represents a small amount of energy in the system. Figure 4 (left) shows the relative energy contained in each mode of the system. For this example, 150 modes were chosen. The order r of this model was selected based on the model fit error (14) plotted in Figure 4 (right). If the order of the model was chosen based on retaining 99% of the energy in the POD modes, almost all of the modes would have been used to construct the IOROM. Instead, the order of the model was chosen based on the model fit error, which indicates that the model performance does not get significantly better after 150 modes. In fact, by including more modes, the IOROM may be overfitting to the nonlinearities of the system which may degrade the performance of the model.

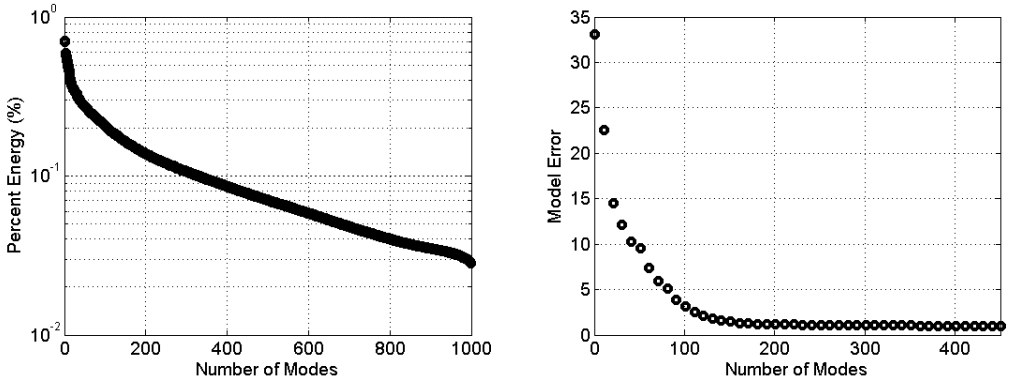

Figure 4. (Left) Percent energy of each mode in the SOWFA simulation. (Right) Model error computed based on the number of modes used to identify a model of the system.

The results of the IOROM can be seen in Figure 5. Specifically, the full flow field is computed from the results of the reduced-order model using (12). The full flow field is shown to demonstrate the capability of the reduced-order model to capture the dominant structures of the flow field, see the top plot in Figure 5. By only selecting 150 modes, this reduced-order model will not be able to capture the high frequency spatial turbulence. In addition to the reconstruction, the input-output behavior was examined. Specifically, the bottom plot of Figure 5 shows the output of the 150 state IOROM and it can be seen that the input-output behavior of the system is retained.

Lastly, the IOROM was applied to a set of validation data to verify that the identified model would work under similar wind conditions but with a different forced input. The same inflow fields were used in both cases. In addition, the same IOROM that was used in Figure 5 is used with the validation data. Although the same inflow conditions are used, the turbulence generated by the upstream turbine will be different due to the different input. The inputs to the upstream turbine can be seen in the third and fourth plots in Figure 6. A Kalman filter (as described in Section 3) is implemented to handle the influence of this change in turbulence. Specifically, the filter parameters were set to $P_0^+ = I_r$, $Q_k = I_r$, and $R_k = 0.001 I_{n_y}$. These matrices were obtained by tuning them to the data set. Figure 6 shows that this IOROM is able to similarly reconstruct the dominant characteristics of the flow provided in the validation case. The results in Figure 6 indicate that this reduced-order model can be used as a predictive model for another similar data set. The power output was also examined to ensure that the input-output behavior is retained with this reduced-order model. The bottom plot of Figure 6 shows the output of the full-order SOWFA simulation and the reduced-order model. Again, the reduced-order model shows good agreement with the full-order simulation. This indicates that this reduced-order model is capable of predicting the output in similar scenarios which makes this model useful for control.

As mentioned previously, it is important to carefully choose the order of the model. If the IOROM is overfit to the data, the IOROM with the Kalman filter will not be able to predict other data sets, i.e. the Kalman gain of the Kalman filter will be large in an attempt to fit the estimated states with the measured outputs. Figure 7 shows the implications of selecting a 300 mode model. Although the input-output behavior is maintained (bottom plot), it can be seen that the reduced-order states (represented in the top plot) no longer represent the dominant dynamics of the system.

6. CONCLUSIONS AND FUTURE WORK

The IOROM method was applied to a high-fidelity wake model. This approach takes advantage of characterizing the dominant dynamics in the flow and provides a low-order approximation of the flow. Using this low-order approximation, a reduced-order model can be constructed that retains the input-output behavior seen in the full-order model. In addition, this

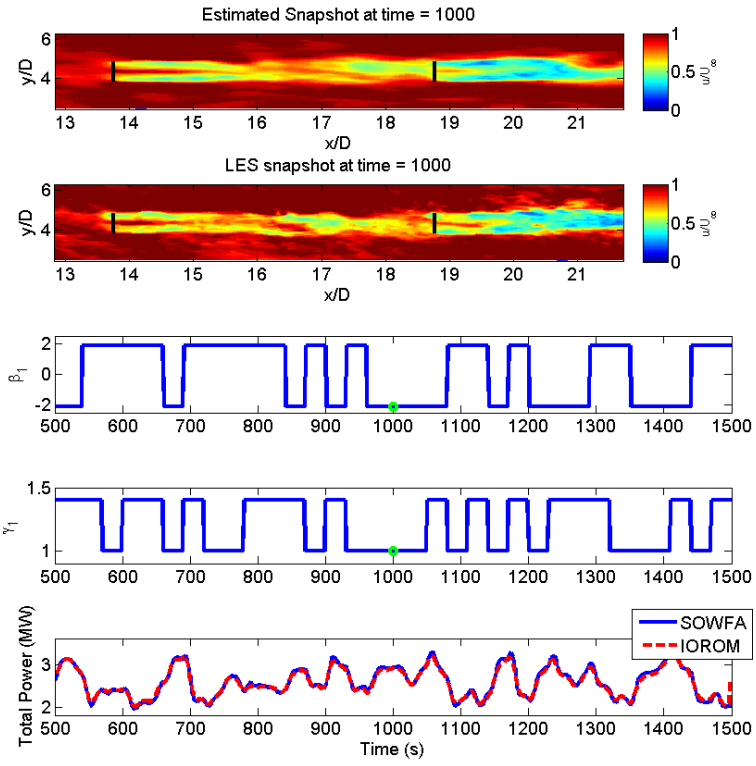

Figure 5. Flow reconstructed using the reduced-order model (top) and compared to SOWFA (second plot). The third and fourth plot show the inputs at the upstream turbine. Lastly, the bottom plot shows the output of the reduced-order model compared to the output of SOWFA.

reduced-order model has a low computational cost and contains the necessary dynamics that are important for problems such as wind farm control. In the example presented in this paper, the IOROM constructed was used on different data sets to demonstrate their predictive capabilities, which could be useful for control design and analysis in wind farms.

7. ACKNOWLEDGMENTS

This work was supported by the National Science Foundation under Grant No. NSF-CMMI-1254129 entitled CAREER: Probabilistic Tools for High Reliability Monitoring and Control of Wind Farms. The first author gratefully acknowledges the financial support from University of Minnesota through the 2015-16 Doctoral Dissertation Fellowship. The authors acknowledge Michele Guala and Kevin Howard for collaborating on the experimental data. Lastly, this work was supported by the U.S. Department of Energy under Contract No. DE-AC36-08GO28308 with the National Renewable Energy Laboratory. Funding for the work was provided by the DOE Office of Energy Efficiency and Renewable Energy, Wind and Water Power Technologies Office. The authors are solely responsible for any omission or errors contained herein.

REFERENCES

1. R. Wiser, “Renewable portfolio standards in the United States - a status report with data through 2007,” LBNL-154E, Lawrence Berkeley National Laboratory, 2008.
2. K. E. Johnson and N. Thomas, “Wind farm control: addressing the aerodynamic interaction among wind turbines,” in *American Control Conference (ACC)*, pp. 2104–2109, IEEE, 2009.

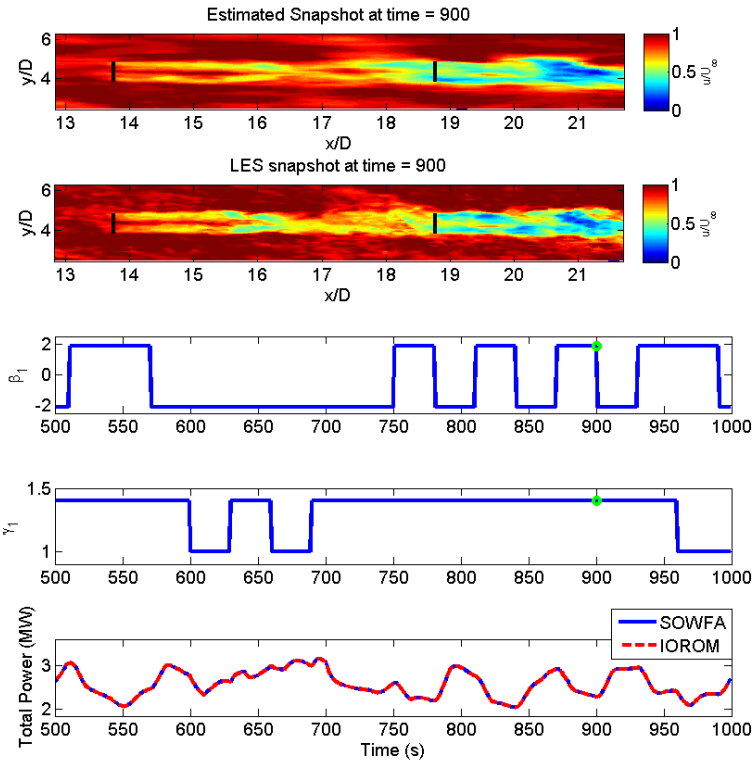

Figure 6. The model was validated using a different data set. The corresponding results are shown here. Flow reconstructed using the reduced-order model (top) and compared to SOWFA (second plot). The third and fourth plot show the inputs at the upstream turbine. Lastly, the bottom plot shows the output of the reduced-order model compared to the output of SOWFA.

3. N. O. Jensen, "A note on wind generator interaction," Tech. Rep. Risø-M-2411, Risø, 1983.
4. R. J. Stevens, D. F. Gayme, and C. Meneveau, "Coupled wake boundary layer model of wind-farms," *Journal of renewable and sustainable energy*, vol. 7, no. 2, p. 023115, 2015.
5. P. Gebraad, F. Teeuwisse, J. Wingerden, P. Fleming, S. Ruben, J. Marden, and L. Pao, "Wind plant power optimization through yaw control using a parametric model for wake effectsa cfd simulation study," *Wind Energy*, vol. 19, no. 1, pp. 95–114, 2016.
6. M. Churchfield and S. Lee, "NWTC design codes-SOWFA," 2012.
7. X. Yang, F. Sotiropoulos, R. J. Conzemius, J. N. Wachtler, and M. B. Strong, "Large-eddy simulation of turbulent flow past wind turbines/farms: the virtual wind simulator (VWiS)," *Wind Energy*, vol. 18, no. 12, pp. 2025–2045, 2015.
8. P. A. Fleming, P. M. Gebraad, S. Lee, J.-W. van Wingerden, K. Johnson, M. Churchfield, J. Michalakes, P. Spalart, and P. Moriarty, "Evaluating techniques for redirecting turbine wakes using SOWFA," *Renewable Energy*, vol. 70, pp. 211–218, 2014.
9. P. M. Gebraad, J. J. Thomas, A. Ning, P. A. Fleming, and K. Dykes, "Maximization of the annual energy production of wind power plants by optimization of layout and yaw-based wake control," 2016.
10. J. Annoni, P. M. Gebraad, A. K. Scholbrock, P. A. Fleming, and J.-W. v. Wingerden, "Analysis of axial-induction-based wind plant control using an engineering and a high-order wind plant model," *Wind Energy*, 2015.
11. J. P. Goit and J. Meyers, "Optimal control of energy extraction in wind-farm boundary layers," *Journal of Fluid Mechanics*, vol. 768, pp. 5–50, 2015.
12. D. Bastine, B. Witha, M. Wächter, and J. Peinke, "Towards a simplified dynamic wake model using POD analysis," *arXiv preprint arXiv:1409.1150*, 2014.
13. P. Holmes, J. Lumley, and G. Berkooz, *Turbulence, Coherent Structures, Dynamical Systems and Symmetry*. Cambridge University Press, 1988.

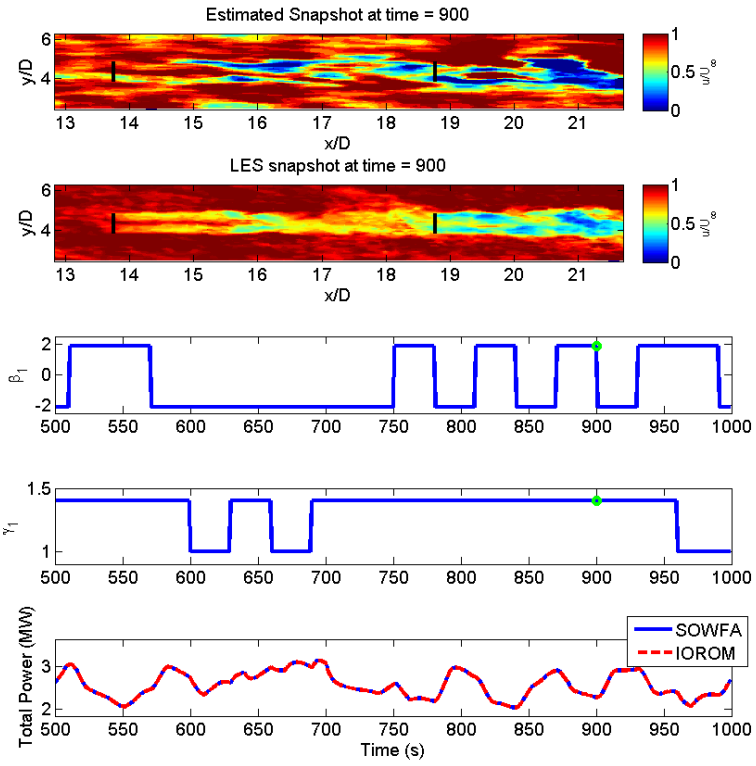

Figure 7. This figure shows an example of a IOROM that was overfit to the original data. The model used in this example had 300 states. When trying to use this IOROM (along with a Kalman filter) with a different data set, the input-output relationship is retained (bottom plot) but the reduced-order states are no longer able to represent the full-order spatial dynamics of the simulation.

14. M. Loéve, *Probability Theory*. Van Nostrand, 1955.
15. J. Beranek, L. Nicolai, M. Buonanno, E. Burnett, C. Atkinson, B. Holm-Hansen, and P. Flick, "Conceptual design of a multi-utility aeroelastic demonstrator," in *13th AIAA/ISSMO Multidisciplinary Analysis Optimization Conference*, pp. AIAA–2010–9350, 2010.
16. P. Schmid, "Dynamic mode decomposition of numerical and experimental data," *Journal of Fluid Mechanics*, vol. 656, pp. 5–28, 2010.
17. P. Schmid, L. Li, M. Juniper, and O. Pust, "Applications of the dynamic mode decomposition," *Theoretical and Computational Fluid Dynamics*, vol. 25, pp. 249–259, 2010.
18. J. Tu, C. Rowley, D. Luchtenburg, S. Brunton, and J. Kutz, "On dynamic mode decomposition: Theory and applications," *submitted to the Journal of Computational Dynamics*, 2013.
19. V. Thomas, C. VerHulst, C. Meneveau, and D. Gayme, "Dynamic mode decomposition analysis of wind turbine wakes," *Bulletin of the American Physical Society*, vol. 60, 2015.
20. K. Willcox and J. Peraire, "Balanced model reduction via the proper orthogonal decomposition," *AIAA journal*, vol. 40, no. 11, pp. 2323–2330, 2002.
21. C. Rowley, "Model reduction for fluids using balanced proper orthogonal decomposition," *International Journal of Bifurcation and Chaos*, vol. 15, no. 03, pp. 997–1013, 2005.
22. J. Proctor, S. Brunton, and J. Kutz, "Dynamic mode decomposition with control," *arXiv:1409.6358*, 2014.
23. M. Viberg, "Subspace-based methods for identification of linear time-invariant systems," *Automatica*, vol. 31, no. 12, pp. 1835–1851, 1995.
24. J. Annoni and P. Seiler, "A method to construct reduced-order parameter varying models," *Submitted to International Journal of Robust and Nonlinear Control*, 2015.
25. B. Danowsky, T. Lieu, and A. Coderre-Chabot, "Control oriented aeroservoelastic modeling of a small flexible aircraft using computational fluid dynamics and computational structural dynamics," in *Proceedings of the AIAA SciTech*

Conference, San Diego, CA, 2016.
26. J. Annoni, P. Gebraad, and P. Seiler, "Wind farm flow modeling using input-output dynamic mode decomposition," in *accepted at the American Control Conference (ACC)*, IEEE, 2016.
27. J. Dean and S. Ghemawat, "Mapreduce: simplified data processing on large clusters," *Communications of the ACM*, vol. 51, no. 1, pp. 107–113, 2008.
28. R. E. Kalman, "A new approach to linear filtering and prediction problems," *Journal of basic Engineering*, vol. 82, no. 1, pp. 35–45, 1960.
29. D. Simon, *Optimal state estimation: Kalman, H infinity, and nonlinear approaches*. John Wiley & Sons, 2006.
30. P. M. Gebraad, P. A. Fleming, and J. van Wingerden, "Wind turbine wake estimation and control using floridyn, a control-oriented dynamic wind plant model," in *American Control Conference (ACC), 2015*, pp. 1702–1708, IEEE, 2015.
31. G. Iungo, C. Santoni-Ortiz, M. Abkar, F. Porté-Agel, M. Rotea, and S. Leonardi, "Data-driven reduced order model for prediction of wind turbine wakes," in *Journal of Physics: Conference Series*, vol. 625, p. 012009, IOP Publishing, 2015.
32. J. Jonkman, "NWTC design codes - FAST," `https://nwtc.nrel.gov/FAST`, 2010.
33. P. Fleming, P. M. Gebraad, S. Lee, J.-W. Wingerden, K. Johnson, M. Churchfield, J. Michalakes, P. Spalart, and P. Moriarty, "Simulation comparison of wake mitigation control strategies for a two-turbine case," *Wind Energy*, 2014.
34. J. M. Jonkman, S. Butterfield, W. Musial, and G. Scott, "Definition of a 5-mw reference wind turbine for offshore system development," 2009.
35. T. Burton, D. Sharpe, N. Jenkins, and E. Bossanyi, *Wind energy handbook*. John Wiley & Sons, 2001.